Chapter 5

Synergistic tribo-activity of nanohybrids of zirconia/cerium-doped zirconia nanoparticles with nano lamellar reduced graphene oxide and molybdenum disulfide

Zirconia in the tetragonal phase is a hard, wear-resistant material with high chemical stability and adorable load-bearing capacity [Philip et al. (2016)]. Mixed-metal oxide nanopowders containing ceria-zirconia and alumina have been reported for catalytic activities [Kim et al. (2009)]. Philip et al. (2016) have studied surface morphology and stability analysis of ceria-zirconia hybrid nanoparticles. Based on XRD results, they have proposed an fcc-fluorite structure and suggested their application as a lubricant additive. For the furtherance of wear resistance and load-bearing capacity of zirconia, an attempt may be made to stabilize the same phase by doping with ceria. Since the drastic reduction in friction and wear has been claimed in the case of graphene supplemented with ceria [Bai et al. (2014) or zirconia [Zhou et al. (2015), it appealed us to prepare cerium doped zirconia nanoparticles using the auto-combustion method [Verma et al. (2019)]. Thus, nanoparticles were prepared, and the existence of the tetragonal phase was identified by their X-ray diffraction patterns [Li et al. (2017), Philip et al. (2016). These nanoparticles have been used for preventing agglomeration and restacking of rGO.

MoS_2 possesses a hexagonal close-packed structure in which each molybdenum atom is covalently bonded to six sulfur atoms in a trigonal prismatic fashion. The presence of weak van der Waals forces between molecular S-Mo-S tri-layers facilitates interlayer slippage. MoS_2 and graphene nanosheets or their nanocomposites have been used very often as oil additives for enhanced lubrication [Song et al. (2018), Xu et al. (2017), Song et al. (2017)]. Xu et al. (2017) have observed synergic tribological behavior of MoS_2 and graphene dispersed in esterified bio-oil. The tribological activity of hydrothermally synthesized

composite, MoS_2-graphene oxide, has been reported by Song and co-workers [Song et al. (2017)]. Wu and his associates have investigated tribological properties of the chemically capped zinc borate/ MoS_2 nanocomposite in oil and grease [Wu et al. (2018a), Wu et al. (2018b)]. Tribological behaviour of Fe_3O_4/MoS_2 nanocomposite in water/oil was studied by Zheng et al. (2016)]. Recently, Fe_3O_4/MoS_2 nanocomposite has been reported to show enhanced lubricating properties in base oils together with significant photocatalytic degradation [Liu et al. (2018)]. The nanocomposite of WS2 with graphene has been reported to yield better tribological results than its constituents [Zheng et al. (2017)]. It was thought to add up the effect of doped nanoparticles, rGO, and MoS_2 together in the form of a tailor-made nanocomposite to obtain captivating tribo-performance. Molybdenum disulfide nanosheets have been prepared by hydrothermal method using ammonium heptamolybdate [Liu et al. (2018)]. The nanohybrids were prepared to have the accretive effect of zirconia/cerium doped zirconia, reduced graphene oxide, molybdenum disulfide on the enhancement of lubrication.

As-prepared nanoparticles, nanosheets, and nanohybrids were characterized by scanning electron microscopy/high-resolution scanning electron (SEM/HR-SEM), energy dispersive X-ray analysis (EDX), powder X-ray diffraction (XRD), Fourier Transform infrared microscopy (FTIR), Raman, electronic (UV-visible) spectroscopy.

Chapter 5

5.1. Materials and Methods

5.1.1. Chemical and Reagents

Extra pure $ZrO(NO_3)_2H_2O$, $Ce(NO_3)_36H_2O$, $(NH_4)_6Mo_7O_{24}4H_2O$, $SC(NH_2)_2$, and citric acid were obtained from Sigma-Aldrich.

5.1.2. Synthesis of Nanoadditives

5.1.2.1. Preparation of Zirconia and Cerium-Doped Zirconia Nanoparticles

Synthesis of ZrO_2 and 10, 20, 30% cerium doped ZrO_2 nanoparticles ZCO-1, ZCO-2, and ZCO-3, respectively, were carried out by auto-combustion method [Verma et al. (2019)]. For the preparation of ZrO_2, at first, a homogeneous aqueous solution of $ZrO(NO_3)2H_2O$ and (7.54g) and citric acid (3.76 g) was made in 30 ml of distilled water. It was heated at nearly 230 °C with continuous stirring to yield the gel.Further heating of the gel results in the formation of ash. The blackish ash was calcined at 500 °C in a muffle furnace for 2h to yield ZrO_2 nanoparticles. Similarly, 10, 20, 30% cerium doped zirconia ZCO-1, ZCO-2, ZCO-3, nanoparticles have been synthesized by adding the required amount of $ZrO(NO_3)_2H_2O$, $Ce(NO_3)_36H_2O$, and citric acid.

5.1.2.2. Preparation of MoS_2 Nanosheets

For the preparation of MoS_2 nanosheets hydrothermal method was used [Wu et al. (2018)]. At first, $(NH_4)_6Mo_7O_{24}4H_2O$ (2.40g) and $SC(NH_2)_2$ (5.20 g) were dissolved in 80 mL of

distilled water by ultrasonication for 30 min to get a uniform solution. The prepared solution was poured into a 200 mL Teflon autoclave, and the temperature was adjusted to 180 °C for 12 h. The formed product was cooled down to room temperature (RT). It was washed by a water-ethanol mixture and dried in a vacuum oven at 60°C.

5.1.2.3. Preparation of Binary Composites of ZrO_2/ZCO-2 with rGO

The ZrO_2 nanoparticles (700 mg) and rGO nanosheets (467 mg) were dispersed in 100 mL ethanol separately by using an ultrasonicator for 1h at RT. The dispersions were intermingled by continuous stirring and sonicated at 70 °C. The mixture was kept for 5 min in the microwave oven at 700 W to yield the black color product [Liu et al. (2018)]. The binary nanocomposite ZCO-2/rGO was synthesized by the same methodology.

5.1.2.4. Preparation of Ternary Composites of ZrO_2/ZCO-2, rGO, and MoS_2

Molybdenum disulfide, 700 mg, was dispersed in 100 mL of ethanol. The prepared dispersion was added to the mixture of ZrO_2/ZCO-2 and rGO. The ternary composites were prepared from this reaction mixture following the same procedure as that for binary composites.

Schematic representation for the procedure of synthesis of ZCO-2/rGO/MoS_2 nanohybrid is shown in **Fig. 5.1**.

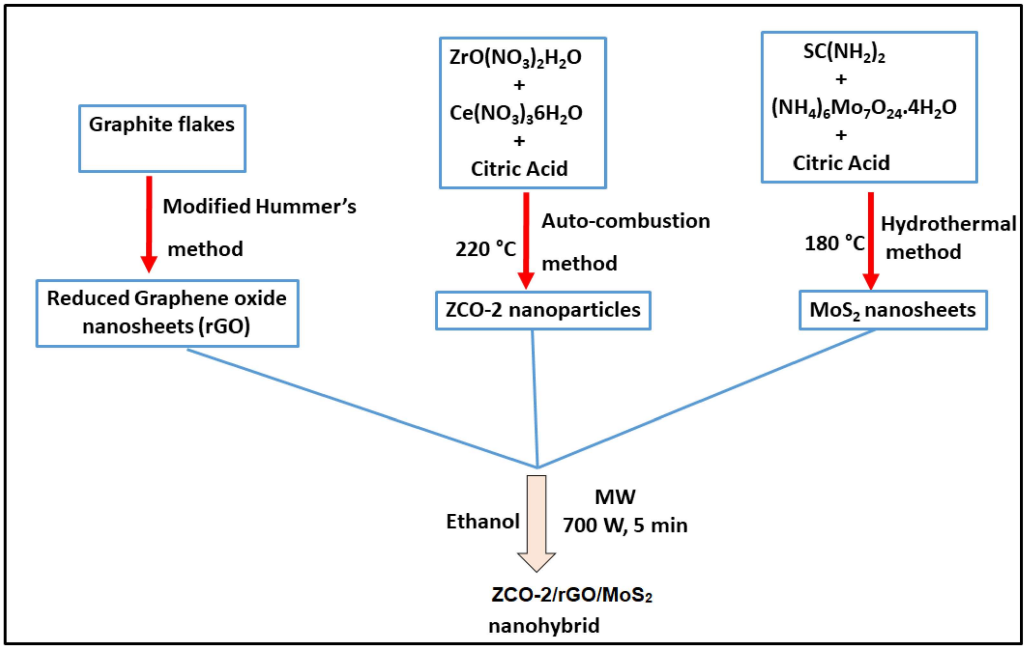

Fig. 5.1. Schematic representation for the procedure of synthesis of ternary nanohybrid ZCO-2/rGO/MoS_2.

5.2. Sample Preparation

The blends of paraffin oil with the studied additives were prepared in various concentrations, 0.0625, 0.1250, 0.1875, and 0.2500 % (w/v) by sonicating at RT for 1h. As per test results, the concentration of 0.125% w/v was found to be the optimized concentration. The tribological tests, therefore, have been conducted at 0.125% w/v concentration of all the additives in base lube; MoS_2, rGO, ZrO_2, ZCO-1, ZCO-2, ZCO-3, ZrO_2/rGO, ZCO-2/rGO, ZrO_2/rGO/MoS_2, and ZCO-2/rGO/MoS_2.

5.3. Results and Discussion

5.3.1. Characterization of Additives

The Characterization of synthesized nanoparticles zirconia/ cerium doped zirconia ZCO-2, their corresponding nanohybrids with reduced graphene oxide, (ZrO_2/ ZCO-2/rGO) and ternary nanohybrids including molybdenum disulfide, (ZrO_2/ ZCO-2/rGO/MoS_2) have been successfully brought about by XRD, FTIR, UV/visible, Raman, TEM/HR-TEM, SEM/HR-SEM, and XPS techniques.

The HR-SEM images of rGO nanosheets, ZCO-2 nanoparticles, the nanohybrid ZCO-2/rGO, MoS_2 nanosheets, and the ternary nanohybrid, ZCO-2/ rGO/MoS_2 are presented in **Fig. 5.2a**, **2b**, **2c**, **2d,** and **2e,** respectively. **Fig. 5.2a** exhibits a lamellar structure for rGO [Jaiswal et al. (2016), Verma et al. (2019)]. The crumpled and transparent sheets of rGO with folded edges are visible. **Fig. 5.2b** shows ZCO-2 nanoparticles of almost spherical shape. However, a slight agglomeration of the nanoparticles can be seen. **Fig. 5.2c** presents the graphene sheet adorned with ZCO-2 nanoparticles. Its EDX Elemental mapping is provided in **Fig. 5.3(a)** to show the distribution of ZCO-2 NPs on rGO nanosheets. The EDX spectrum of ZCO-2/rGO (not given here for the sake of brevity) shows elemental composition. The presence of clearly visible peaks assignable to zirconium, cerium, and oxygen in addition to carbon is indicative of the formation of the proposed nanohybrid. **Fig. 5.2d** displays nanosheets of MoS_2 while **Fig. 5.2e** illustrates MoS_2 nanosheets attached on rGO layers, and ZCO-2 nanoparticles are decorated over them. The EDX spectrum of the ternary nanohybrid

provides perspicuous signals for the elements molybdenum and sulfur in addition to zirconium, cerium, oxygen, and carbon. The depicted wt% data in **Fig. 5.2e$_1$** endorses the formation of ternary nanohybrids. EDX elemental mapping has been given in **Fig. 5.3(b)** to differentiate rGO, MoS_2, and ZCO-2 in the nanocomposite.

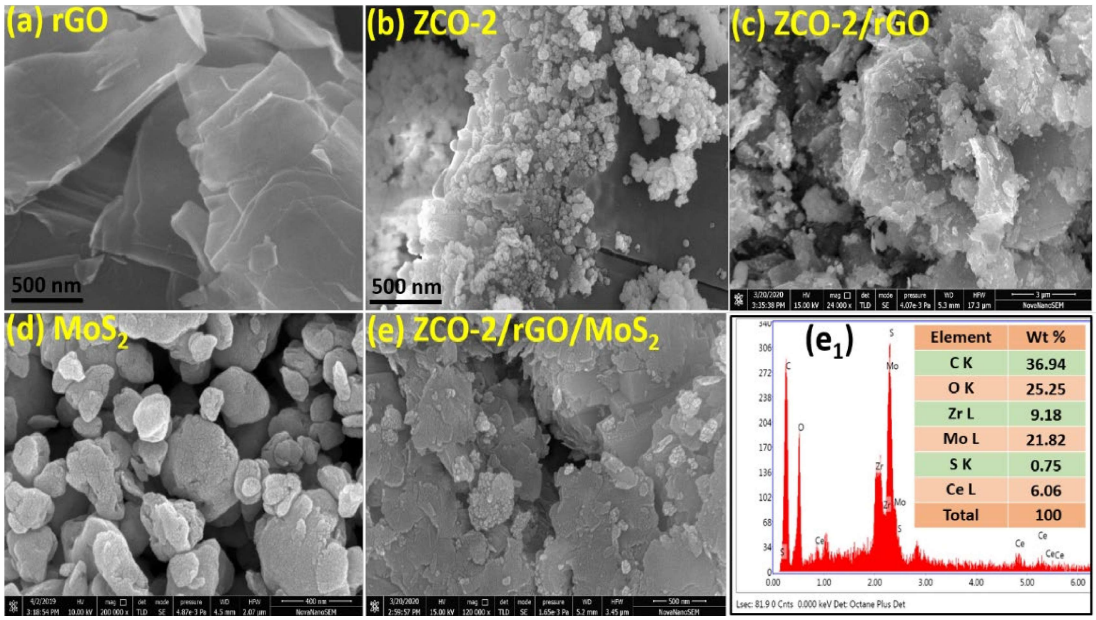

Fig. 5.2. HR-SEM images of (a) rGO, (b) ZCO-2, (c) ZCO-2/rGO, (d) MoS_2 and (e) ZCO-rGO/MoS_2 with its EDX spectrum (e_1).

For a deeper understanding of morphological characteristics, TEM images of the studied nanomaterials have also been recorded and displayed in **Fig. 5.4**, ZrO_2 (a), rGO (b), ZCO-2 (c), MoS_2 (d) ZCO-2/rGO (e), and ZCO-2/rGO/MoS_2 (f) respectively.

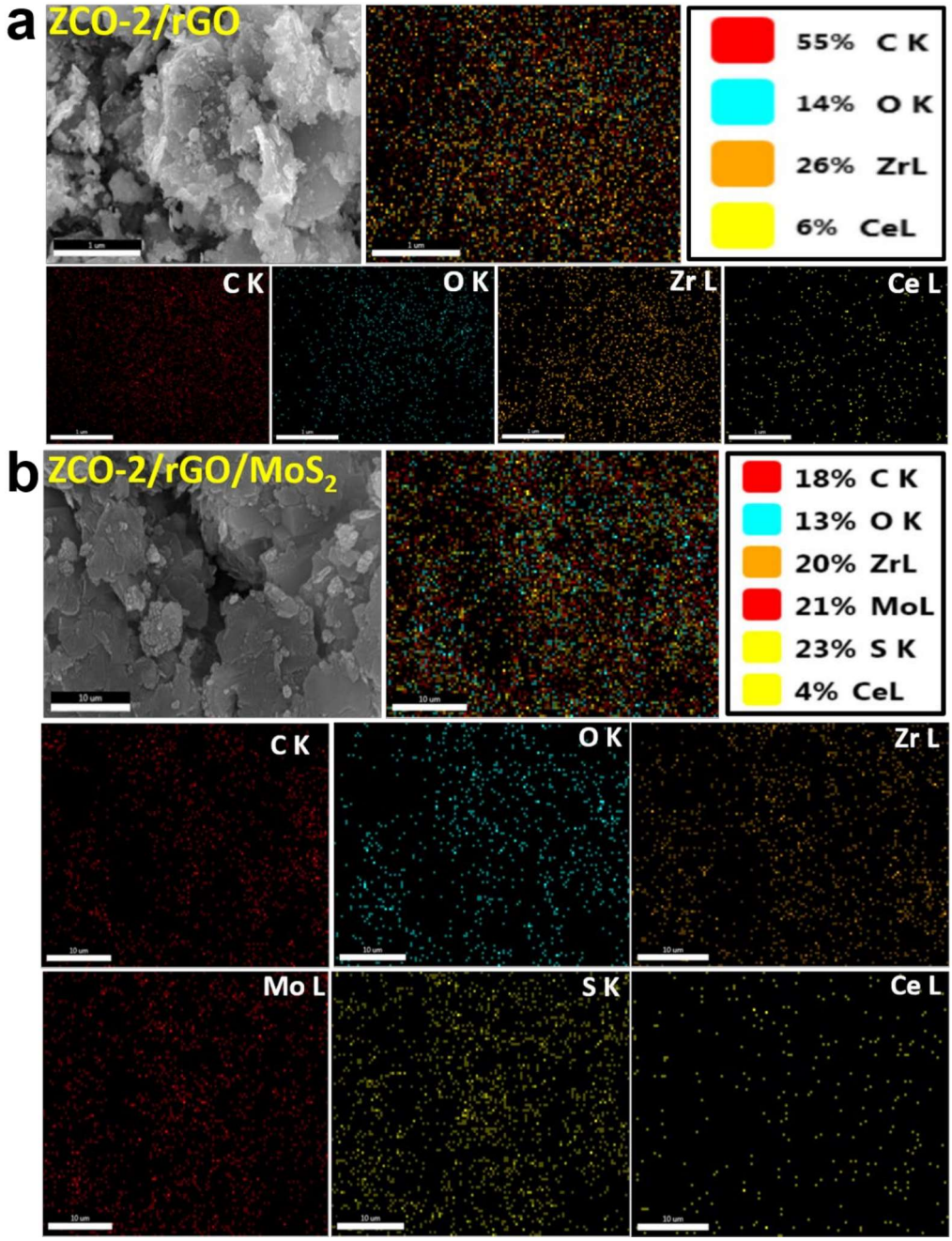

Fig. 5.3. EDX elemental mapping of **(a)** ZCO-2/rGO, and **(b)** ZCO-2/rGO/MoS_2 nanomaterials.

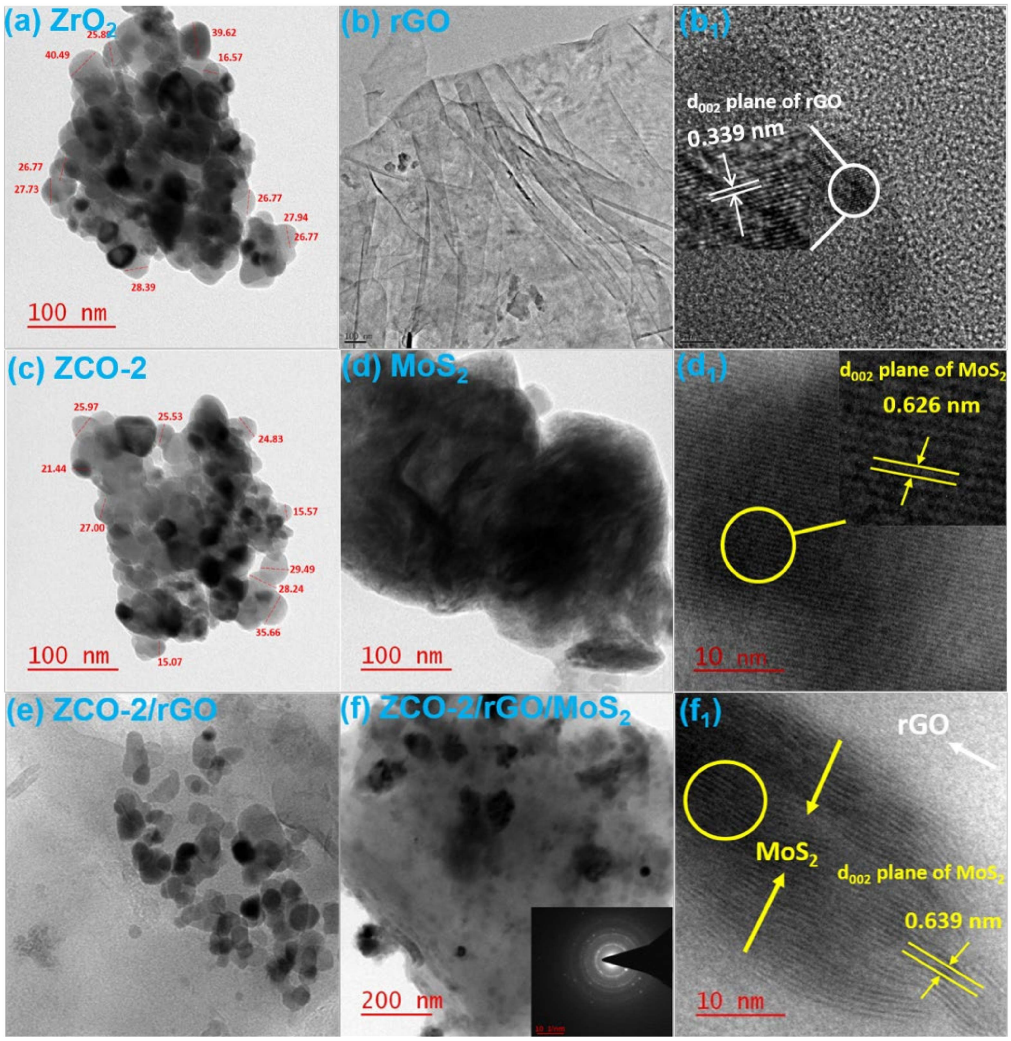

Fig. 5.4. TEM images of (a) ZrO_2, (b) rGO, (c) ZCO-2, (d) MoS_2, (e) ZCO-2/rGO, and (f) ZCO-2/rGO/MoS_2 and HR-TEM images of (b_1) rGO, (d_1) MoS_2, and (f_1) ZCO-2/rGO/MoS_2.

The tetragonal phase of ZrO_2 and ZCO-2 nanoparticles is apparent in the TEM images, **Fig. 5.4a** and **Fig. 5.4c**. The average size of nanoparticles seems to be in the range of 25-30 nm. The lamellar structure of rGO is noticeable from **Fig. 5.4(b)**. The nanosheets appear to be quite transparent, with little folding at the edges. The interlayer distance of the (002) plane

of rGO is obtained as 0.339 nm [Paul et al. (2019), Jaiswal et al. (2016), Verma et al. (2019)]. The HR-TEM image of MoS_2 nanosheets shows a layered structure with weak van der Waals type of forces existing in between the layers. The interlayer distance of the (002) plane, 0.62 nm, is in concurrence with XRD. The findings regarding the microstructure of MoS_2 nanosheets are the same as reported by Rawat et al. [Yi et al. (2018), Rawat et al. (2019)]. However, The TEM and HR-TEM images of the ternary nanohybrids ZCO-2/rGO/MoS_2 reveal that MoS_2 nanosheets are scattered on the surface of rGO. The nanoparticles ZCO-2 gracing the rGO and MoS_2 surfaces are conspicuously visible in **Fig. 5.4(f)**. Presence of sharp, polycrystalline rings along with strong diffraction spots in the selected area diffraction pattern (SAED) of the ternary nanohybrids (shown in the inset of **Fig. 5.4(f)** is indicative of high crystallinity. It is a noticeable feature of HR-TEM **Fig. 5.4(f_1)** that interlayer distance of MoS_2 nanosheets [Yi et al. (2018)] has remarkably enhanced to 0.639 nm in the ternary nanohybrid [Nautiyal et al. (2019)]. Thus it may be inferred that the nanoparticles act as spacers [Paul et al. (2019), Bai et al. (2019), Zhou et al. (2016)] between rGO and MoS_2 layers and alleviate their restacking [Zhang et al. (2017), Song et al. (2019), Yi et al. (2018), Paul et al. (2019), Bai et al. (2014), Zhou et al. (2015)].

Reduction of GO to rGO is apparent as the typical peak of GO appearing around 11° due to (001) reflection disappears in XRD of rGO and the nanohybrids (**Fig. 5.5a**). The diffraction patterns of rGO and the nanohybrids exhibit a broad peak at 24.5° assignable to (002) reflection of rGO [Verma et al. (2019)].

The diffraction pattern of ZrO_2 is indicative of tetragonal crystallites [Li et al. (2017)]. The tetragonal structure continues to exist in cerium-doped zirconia ZCO-1, ZCO-2, and ZCO-3, as apparent from their diffraction patterns. The absence of any additional peak due to cerium confirms that a single tetragonal phase is maintained. As compared to pure zirconia, the intensity of the peaks has reasonably decreased in the case of cerium doped zirconia. However, the diffraction patterns of the nanohybrids ZrO_2/rGO and ZCO-2/rGO show the same peaks but with comparatively much-reduced intensity.

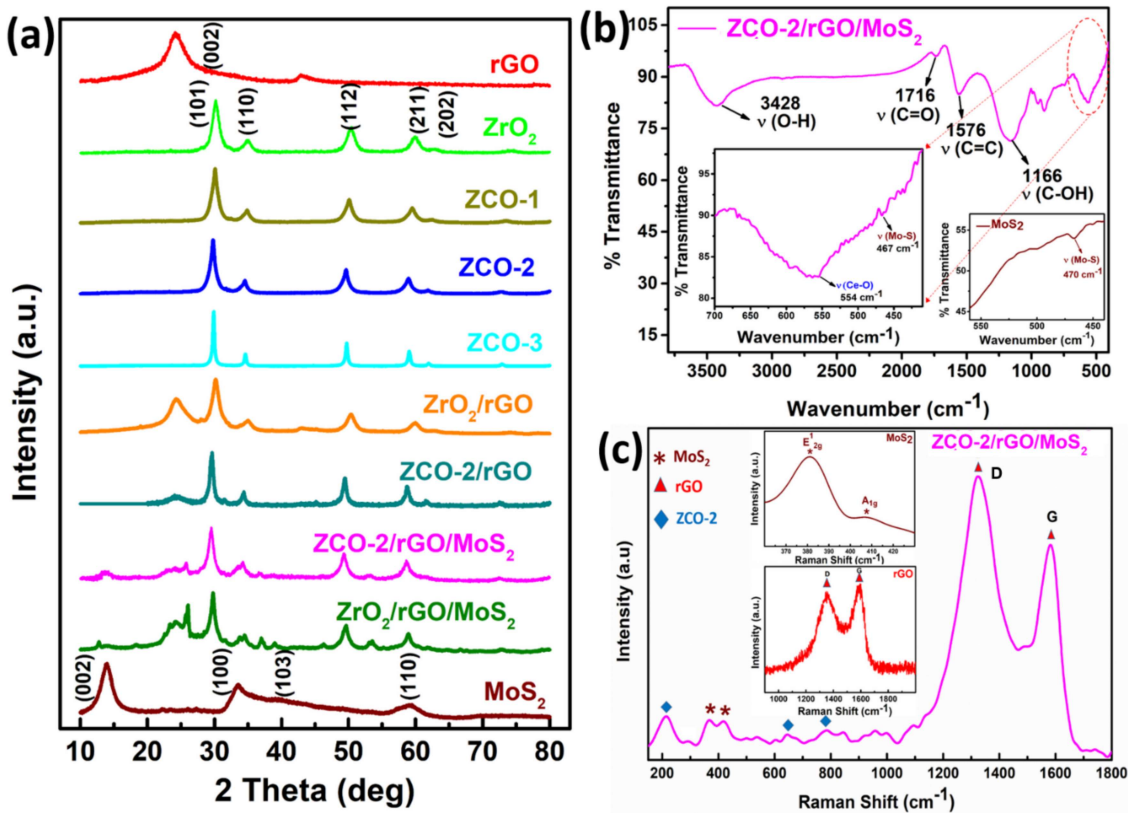

Fig. 5.5 (a) XRD patterns of as-prepared nano additives, **(b)** FTIR, and **(c)** Raman spectra of ternary composite ZCO-2/rGO/MoS_2 (inset showing spectra of MoS_2/rGO).

The XRD pattern of MoS_2 can be indexed to the hexagonal structure as per JCPDS no. 37-1492 and JCPDS 77-1716, showing characteristic peaks at 14.3°, 33.6°, 39.4°, and 59.4° corresponding to (002), (100), (103) and (110) planes respectively [Yi et al. (2018), Zheng et al. (2016)].

The presence of a strong and sharp diffraction peak for the (002) plane conforms to a well-stacked lamellar structure [Yi et al. (2018)]. The d-spacing of the (002) plane is calculated as 0.626 nm, which matches exactly with the TEM analysis [Yi et al. (2018), Rawat et al. (2019)]. The phase structure of MoS_2 is carried as such in the ternary nanohybrids with a difference that the intensity of the peak due to (002) plane is reduced sufficiently. The reduction in intensity indicates that crystallite size and the number of layers along the c axis are reduced in the nanohybrids as compared to MoS_2 nanosheets. The interspacing of (002) plane has exalted in ternary composites to 0.639 nm [Nautiyal et al. (2019), Paul et al. (2019)] indicating components in the hybrid have well interacted with each other.

In the FTIR spectra (**Fig. 5.5b**) of the nanohybrids ZCO-2/rGO/MoS_2, the absorption band due to Ce-O [Philip et al. (2016)] and Mo-S [Rawat et al. (2019)] stretching frequencies are observed around 554 and 467 cm^{-1} besides typical bands of rGO [Zhou et al. (2015)] in the region 1100-1720 cm^{-1}. The presence of these bands validates the formation of the ternary composite.

Raman spectra of rGO and its nanohybrids, employing 785 nm laser excitations, are shown in **Fig.5.5c**. There are two peaks of very high intensity at 1360 and 1582 cm^{-1} in the spectrum

of rGO, which are attributed to D and G bands, respectively [Verma et al. (2019)]. The D band is assignable to the breathing mode of A_{1g} symmetry and provides information about sp^3/sp^2 hybridized defects. The G band is attributed to doubly degenerate phonon mode of E_{2g} symmetry and relates to vibration in the ordered sp^2- hybridized carbon atoms. The intensity ratio of D and G bands I_D/I_G is an important parameter for the interpretation of disorders or defects in the structure. Its value of 0.92 in rGO has increased to 1.34 in ZCO-2/rGO/MoS_2, which may be associated with increased defects in the composite. For MoS_2, E^1_{2g} and A_{1g} bands are observed at 380 and 407 cm^{-1}, respectively [Yi et al. (2018)]. The E^1_{2g} mode corresponds to in layer displacement of molybdenum and sulfur atoms, while the A_{1g} mode relates to out of layer symmetric displacement of sulfur atoms along the c axis. A difference of 27 cm^{-1} between these two modes indicates a multi-layered structure. The blue shift of A_{1g} and decrease of inter-peak separation are significant for decreasing no. of MoS_2 layers. These bands are marked in the Raman spectrum of the ternary nanohybrid. Several bands have also been marked between 200 to 640 nm due to the tetragonal phase of zirconia [Zheng et al. (2016)].

5.3.2. Dispersion Stability of Nanoadditives in Base Oil

For determination of dispersion stability of different blends, absorbance values were recorded in the range 200-800 nm at six-hour intervals starting from zero up to 48 hours using UV/visible spectroscopic technique. The samples for the test were prepared by ten times dilution of the original dispersion containing the additives (0.125% w/v) in paraffin

oil. **Fig. 5.6(a)** illustrates the variation of relative absorbance vs. settling time for all nano additives. In every case, the relative absorbance drops with time, but the dropping is beyond doubt, least for the ternary nanohybrid ZCO-2/rGO/MoS_2 followed by ZrO_2/rGO/MoS_2, then ZCO-2/rGO, ZCO-2, MoS_2, and at last rGO.

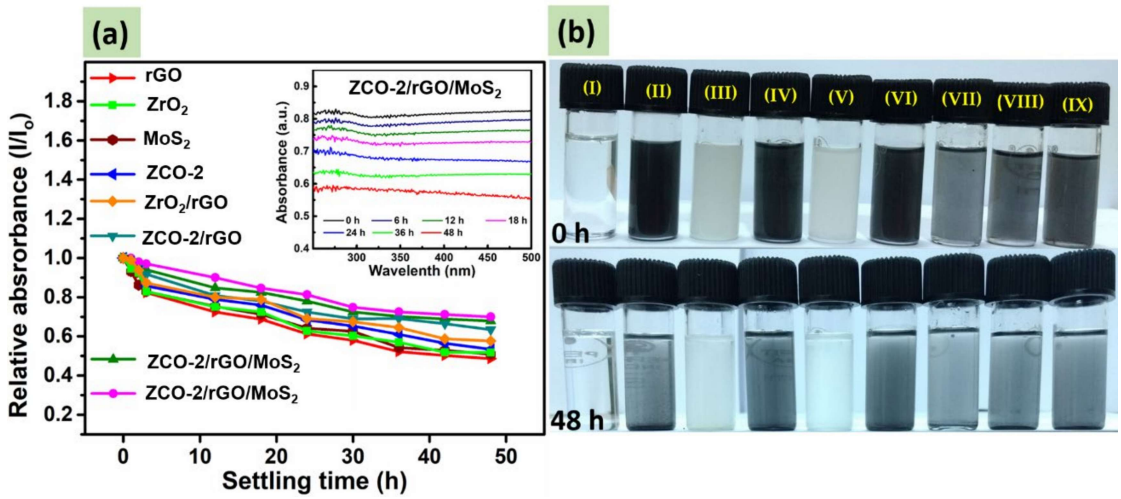

Fig. 5.6.(a) Dispersion stabilities of base oil containing rGO, ZrO_2, MoS_2, ZCO-2, ZrO_2/rGO, ZCO-2/rGO, ZrO_2/rGO/MoS_2, and ZCO-2/rGO/MoS_2 studied by UV-vis spectrophotometry (inset showing a decrease in absorbance of 320 nm band against time). **(b)** Optical photographs of (I) plain PO and PO with dispersed nano additives (II) rGO, (III) ZrO_2, (IV) MoS_2, (V) ZCO-2, (VI) ZrO_2/rGO, (VII) ZCO-2/rGO, (VIII) ZrO_2/rGO/MoS_2, and (IX) ZCO-2/rGO/MoS_2 at zero time and after 48 hours.

Though the most active additive exhibits maximum stability, others also have adequate stability as relative absorbance has dropped down only up to approximately 0.5. The inset of the figure shows the absorbance of ZCO-2/rGO/MoS_2 within 48 hours at 6h intervals. It can be vividly seen that the composite absorbs at 320 nm, and the absorbance

decreases with time from 0.8 to approximately 0.6 within 48 hours. **Fig. 5.6(b)** exhibits the photographs of base oil and its dispersions with the ternary composite at zero time and after 48 hours.

5.3.3. Assessment of Tribological Behaviour

The tests were performed to see the effect of concentration on tribological properties. The different concentrations of additives, starting from blank, 0.0625, 0.1250, 0.1875, and 0.2500% w/v, were tested at a load of 392 N for 60 min test duration in base lube, and corresponding results are displayed in **Fig. 5.7**.

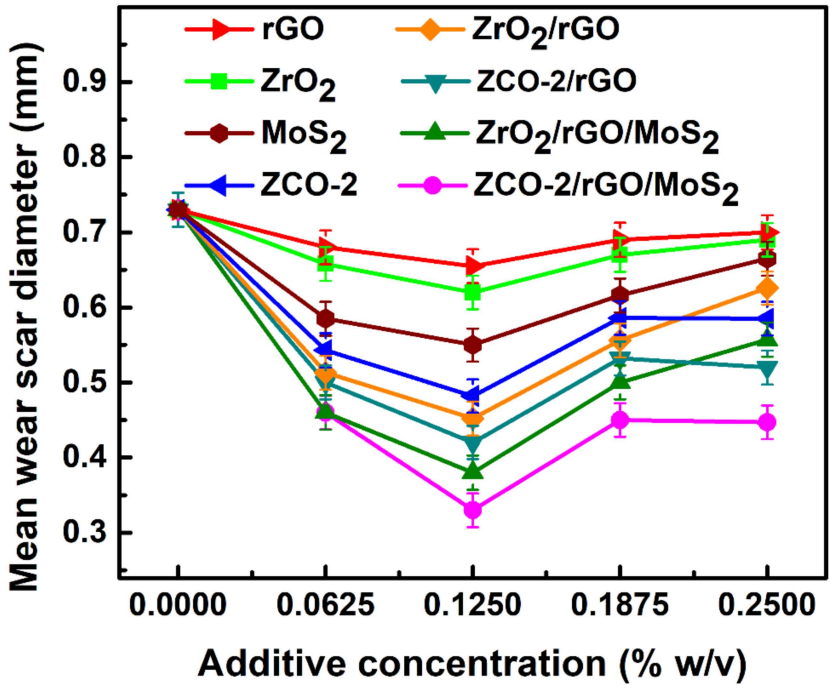

Fig. 5.7. Variation of mean wear scar diameter for the paraffin oil as a function of additive concentration at 392 N applied load for 60 min duration.

It can be easily stated that the tested formulations were found to be tribologically active at all the tested concentrations. At the first test concentration, 0.0625% w/v MWD value for rGO falls off as compared to blank paraffin oil.

For different blends, the values of MWD are further lowered in the order ZrO_2, ZCO-2, MoS_2, followed by binary nanohybrids ZrO_2/rGO, ZCO-2/rGO, and at last ternary nanohybrids ZrO_2/rGO/MoS_2, ZCO-2/rGO/MoS_2. This sequence of diminution of MWD values in the presence of the investigated additives directly relates to the enhancement of their tribo-activity. For the next concentration, 0.1250% w/v, there is a further decline of MWD values for each of the additives, and the same order concerning each other prevails. When concentration is increased to 0.1875% w/v, the MWD values are tangibly increased in each case, although their mutual ordering remains the same. Consequent upon the remarkable increase of MWD values at 0.1875% w/v for all the tested additives, an inference is drawn that 0.1250 %w/v should be taken as the optimized concentration for all the formulations. For the last concentration, 0.2500% w/v, MWD values are more or less stabilized or show a slight increase in some cases.

For assessment of antiwear properties, ASTM D4172 tests of base oil and its admixtures with different additives were conducted using the optimized concentration (0.1250% w/v) at 392 N load for 60 min test duration. The test results are summarized in **Fig. 5.8a.**

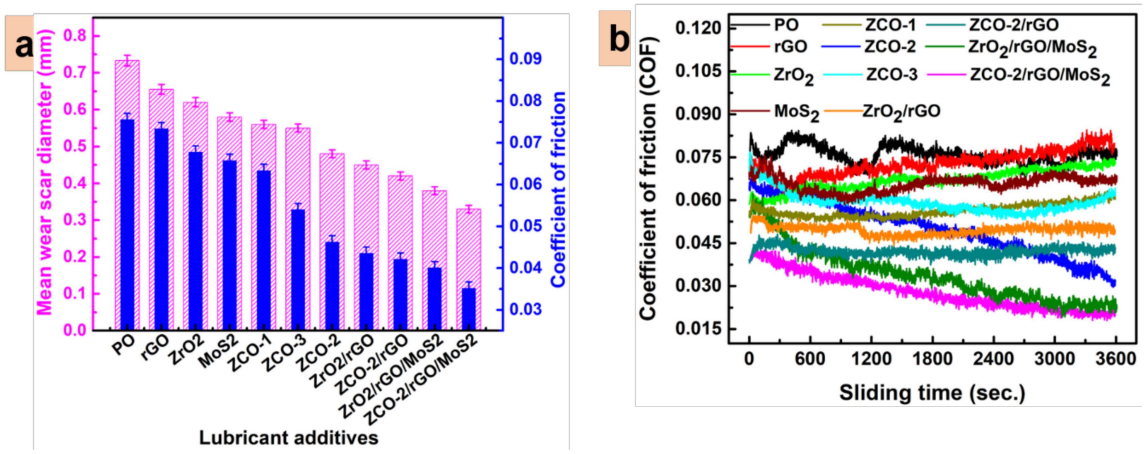

Fig. 5.8. Variation in tribological parameters in the absence and presence of different nano additives (0.125% w/v) in paraffin oil: load, 392 N; sliding speed, 1200 rpm; temperature, 75 °C; sliding duration, 60 min; concentration of additives, 0.125% w/v. **(a)** mean wear scar diameter and the average coefficient of friction **(b)** coefficient of friction as a function of sliding time.

The figure shows the variation of the two most important parameters, mean wear scar diameter (MWD) and the average coefficient of friction (COF), together in the form of a bar diagram. It is clearly perceived from the figure that the base oil shows MWD as 0.733 mm, but in the presence of individual additives, percentage reduction increases gently, like rGO (11%), ZrO_2 (15%), MoS_2 (21%), ZCO-1 (24%), ZCO-3 (25%) and ZCO-2 (35%). The binary composites ZrO_2/rGO and ZCO-2/rGO cause a further increase in % reduction to 39 and 43, respectively. Indubitably, the humongous reduction is observed when ternary nanohybrids are used, ZrO_2/rGO/MoS_2 (48%) and ZCO-2/rGO/MoS_2 (55%). Thus, illustrious antiwear behavior is observed in the case of the ternary composite of rGO and MoS_2 with 20% cerium doped zirconia (ZCO-2).

Likewise, the observed average COF value 0.0756 for plain paraffin oil undergoes an enormous reduction in the presence of different additives following the same order as that of MWD, rGO (3%), ZrO_2 (10%), MoS_2 (13%), ZCO-1 (16%), ZCO-3 (29%) and ZCO-2 (40%), ZrO_2/rGO (42%), ZCO-2/rGO (44%), ZrO_2/rGO/MoS_2 (47%) ZCO-2/rGO/MoS_2 (53%). The huge diminution in MWD and COF values in the presence of the above additives is directly related to their antiwear and antifriction properties, respectively. This kind of behaviour may be interpreted in terms of the crucial role played by different additives in the formation of the tribochemical film (*in situ*), which prevents contact of the proximal surfaces and is indispensable for abatement of their friction and wear. Here nanoparticles as nano bearings and layered structure of rGO and MoS_2 altogether have facilitated the sliding motion, which in turn, has ameliorated the efficiency of composites. Doping of zirconia by cerium has increased the efficiency, which may be ascribed to an increase in several slip planes due to created defects.

The **Fig. 5.8b** portrays variation of COF of mating surface vs. time at 392 N load in plain base lube or its admixtures. It is a very important parameter from the viewpoint of the life expectancy of machines. In general, COF values are initially high in each case; later on, with time as tribofilm is formed, the values are reduced. It is apparent from the figure that the COF is inevitably highest for the PO alone. Its blend with rGO as additive comes next, showing a fair amount of reduction in the COF values at the beginning of the test. However, after a

certain period, little increase in COF values is noted, probably due to slight agglomeration, which makes the surface less protected.

Further reduction in COF is identified when blends with zirconia nanoparticles followed by MoS_2 nanosheets are implied. These nanomaterials are succeeded by doped nanoparticles in terms of reducing COF values. Out of 10, 20, and 30% cerium doped zirconia nanoparticles (ZCO-1, ZCO-2, ZCO-3) as additives, the best results are obtained for ZCO-2 where the minimum values of COF are observed.

Further lowering of COF is visible when formulations consisting of binary composites are incorporated. A comparison of binary composite blends shows that COF is pretty lower and consistent in the case of ZCO-2/rGO than ZrO_2/rGO. Amazing results are noticed when ternary nanocomposites are appended to the base oil. Undoubtedly, ZCO-2/rGO/MoS_2 outperforms ZrO_2/rGO/MoS_2, as discussed above for MWD values. Accordingly, out of all the tested additives, the lowest and stabilized COF is perceived in the case of ZCO-2/rGO/MoS_2.

For determination of wear rate, the test was conducted at 392 N load for 1.5 h duration, and values of MWD were noted after every 15 min test run. As mean wear volume (MWV) is a more justified parameter than MWD for calculation of wear rate, the observed MWD values for different sliding periods have been converted to MWV using a suitable formula [Verma et al. (2019)].

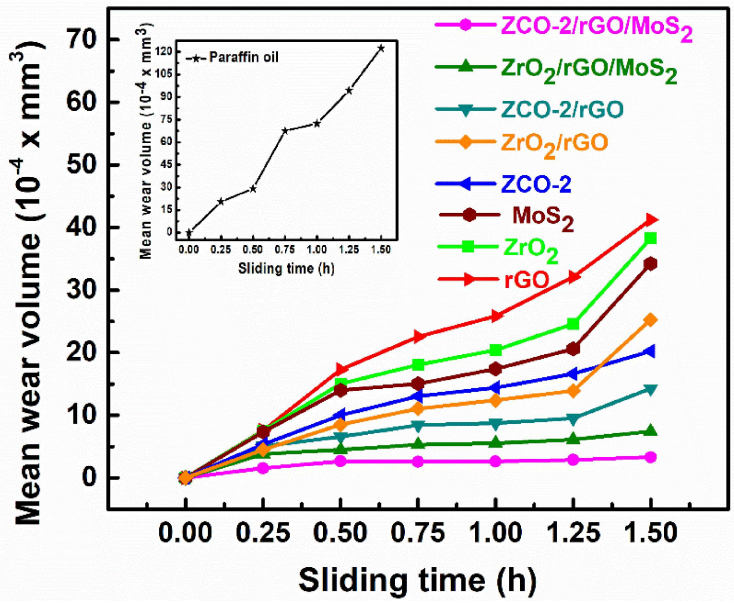

Fig. 5.9. Variation of mean wear volume with sliding time for paraffin oil without (given in inset) and with 0.125% w/v of different nano additives for 1.5 h test duration.

Fig. 5.9 portrays variation of MWV values as a function of sliding time from 0 to 1.5h. The wear rate has been obtained by fitting a linear regression model [Verma et al. (2019)]. The running-in period is taken between 0-0.75 h, while the steady-state period has been considered during 0.75 h onwards.

Running-in and steady-state wear rates have been obtained concerning the above mentioned periods and are depicted in **Fig. 5.10** and **Fig. 5.11**, respectively. The acquired data are presented in **Table 5.1**.

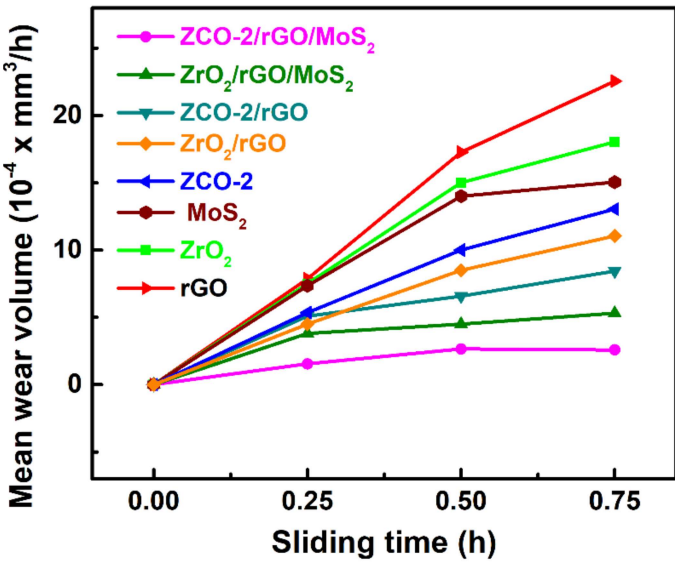

Fig. 5.10. Determination of running-in wear rate by varying mean wear volume with time (h) for paraffin oil containing (0.125% w/v) nano additives at 392 N applied load

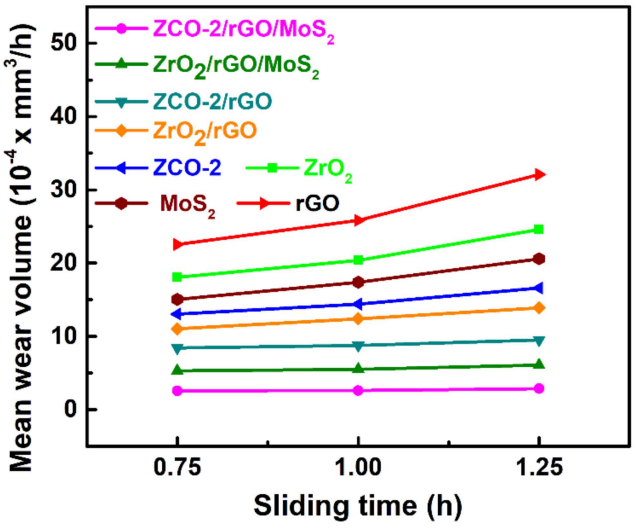

Fig. 5.11. Determination of steady-state wear rate by varying mean wear volume with time (h) for paraffin oil containing (0.125% w/v) nano additives at 392 N applied load.

Table 5.1. Wear-rate for paraffin oil (PO) in the presence and absence of nano additives for 60 min test duration at 392 N applied load

S/N	Lubricants	Wear rate (10^{-4} × mm^3/h)	
		Running-in	Steady-state
1	PO	84.48	53.33
2	rGO	31.07	18.78
3	ZrO_2	24.66	13.08
4	MoS_2	20.72	11.08
5	ZCO-2	17.52	7.08
6	ZrO_2/rGO	14.87	5.68
7	ZCO-2/rGO	10.73	2.14
8	ZrO_2/rGO/MoS_2	6.64	1.60
9	ZCO-2/rGO/MoS_2	3.54	0.59

In the presence of plain base lube, the values of running-in and steady-state wear rates are quite high. However, these values undergo a severe reduction in the presence of blends of base oil with various additives.

The extent of reduction in wear rates for different additives is in tune with their antiwear properties, as discussed above. It is interesting to note that for ZCO-2 alone as an additive, the steady-state wear rate is significantly reduced. From the observed results of wear rates, it may be pleaded authoritatively that both the ternary composites, in general, and ZCO-2/rGO/MoS_2, in particular, prove their potentiality for tribological applications.

For determination of the load-bearing capacity of different admixtures, a step loading test (ASTM D5183) was conducted using the optimized concentration of the additives under the standard conditions of 392 N load, 600 rpm, 75 °C temperature, and 60 min duration, after the termination of the running-in period. The test for the steady-state coefficient of friction was carried out by subsequent increment of 98 N load after every 10 min. The observed data are presented in **Fig. 5.12**.

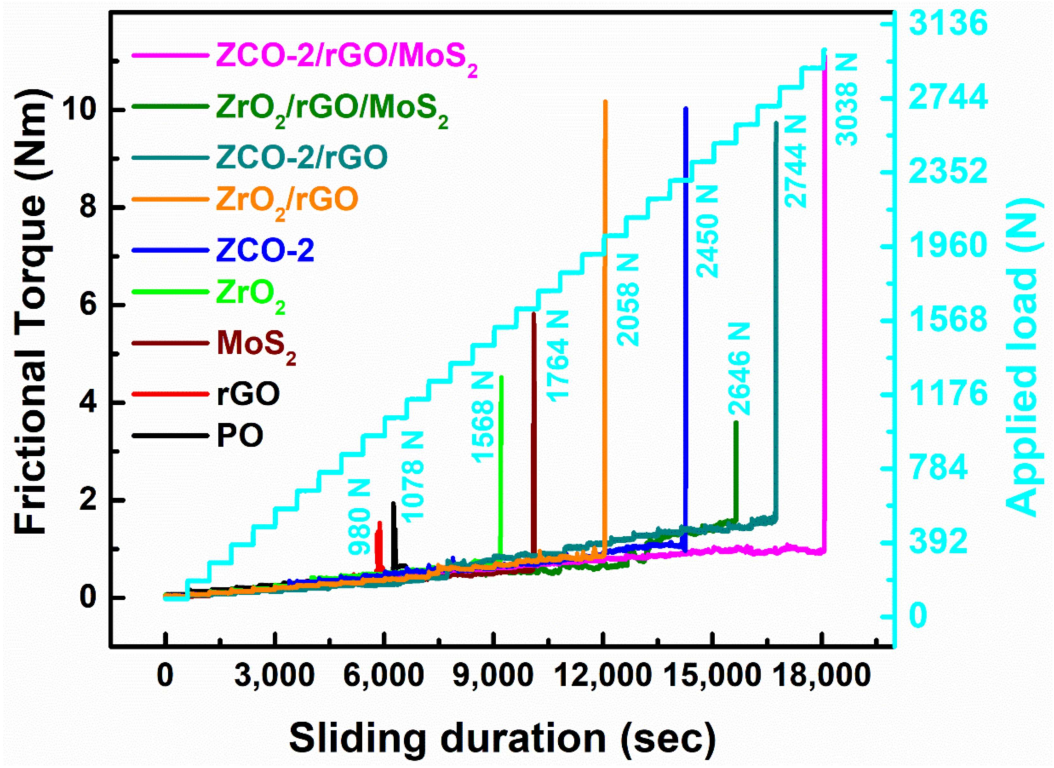

Fig. 5. 12. Variation of frictional torque as a function of stepwise loading and time for PO in absence and presence of different nano additives: sliding speed, 600 rpm; temperature, 75°C; concentration of additives, 0.125% w/v.

In the presence of plain paraffin oil alone, the value of frictional torque is quite high, and seizure of the tribo-pairs occurs at 1078 N. At the seizure load, rupture of tribofilm occurs, which perturbs the steady-state. The lubricant loses its capability to bear the load. With the increase in several increments of load and time together, the frictional torque values have drastically reduced and stabilized for different admixtures at each applied load as compared to the base oil.

It is a noticeable feature of **Fig.5.12** that plain base oil shows seizure load at 1078 N while its admixture with rGO sustains the load only up to 980 N.

This unruly behavior of rGO is attributed to its weaker adhering tendencies. However, blends of base oil with other additives increase the seizure load ZrO_2 (1568 N), MoS_2 (1764 N), ZrO_2/rGO (2058 N), ZCO-2 (2450 N), ZrO_2/rGO/MoS_2 (2646 N), ZCO-2/rGO (2744 N) and finally ZCO-2/rGO/MoS_2 (3038 N). Thus, the presence of MoS_2 and ZrO_2 or ZCO-2 has strengthened rGO, and maximum load-bearing capacity is observed for the ternary composite ZCO-2/rGO/MoS_2.

5.3.4. Morphological Features of the Worn Surface

The surface techniques, SEM and AFM, were employed for studying morphological characteristics of the wear track in the presence of paraffin oil alone or containing the investigated additives at the optimized concentration (0.125% w/v) under standard conditions of ASTM D4172 test. The SEM images for the base lube with or without considered nano additives are displayed in **Fig. 5.13**.

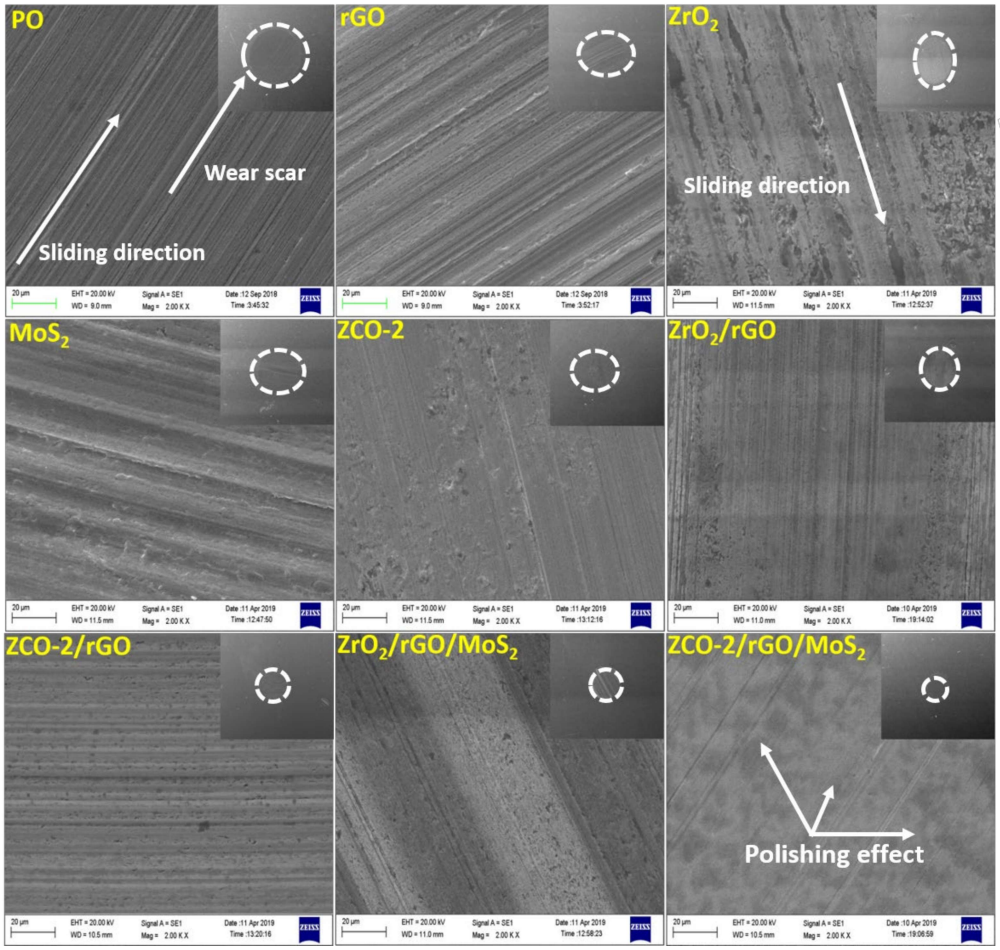

Fig. 5.13. SEM micrographs (inset: full view of wear scar at 100X, wear scar surface at 2.00KX magnification) of the worn steel surface lubricated with paraffin oil with and without different nano additives (0.125% w/v) for 60 min test duration at 392 N applied load.

In the presence of the base lube, the worn surface appears to be corrugated in the SEM images because of dreadful scratches. However, the worn surfaces are smoothened in the presence of the admixtures. The order of smoothening of the worn surfaces corroborates the antiwear properties of the additives. The values of MWD for base lube with or without

additives have been displayed in the inset of each micrograph. The value of MWD 0.733 mm for oil alone, has diminished significantly for its blends with different additives, rGO (0.655mm), ZrO_2 (0.620mm), MoS_2 (0.550mm), ZCO-2 (0.480mm), ZrO_2/rGO (0.450mm), ZCO-2/rGO(0.420mm), ZrO_2/rGO/MoS_2 (0.380mm) and ZCO-2/rGO/MoS_2 (0.330mm)). Descending order of MWD from plain oil through various additives to finally the ternary composite of ZCO-2 is harmonious with the gradual improvement of the surface. The individuals of the nanohybrids have genuinely outperformed their part in achieving smoothness of the contact surfaces. The surface has been mended by the nanoparticles as they are small enough to fill the minute pits or gaps [Paul et al. (2019), Wu et al. (2018)]. The self-lubricating behavior of nanosheets has further advanced as nanoparticles increase their dispersibility by preventing agglomeration [Nautiyal et al. (2019), Song et al. (2019), Paul et al. (2019)].

Morphological characteristics of the surface of the balls after the antiwear test (392 N load, 1h, 1200 rpm, 75 °C) performed in the presence of plain base oil and its blends with the synthesized additives were studied by AFM. The *3D* AFM images of the wear scar surface are presented in **Fig. 5.14**, incorporating surface roughness values [line roughness (Rq) and area roughness (Sq)] as well.

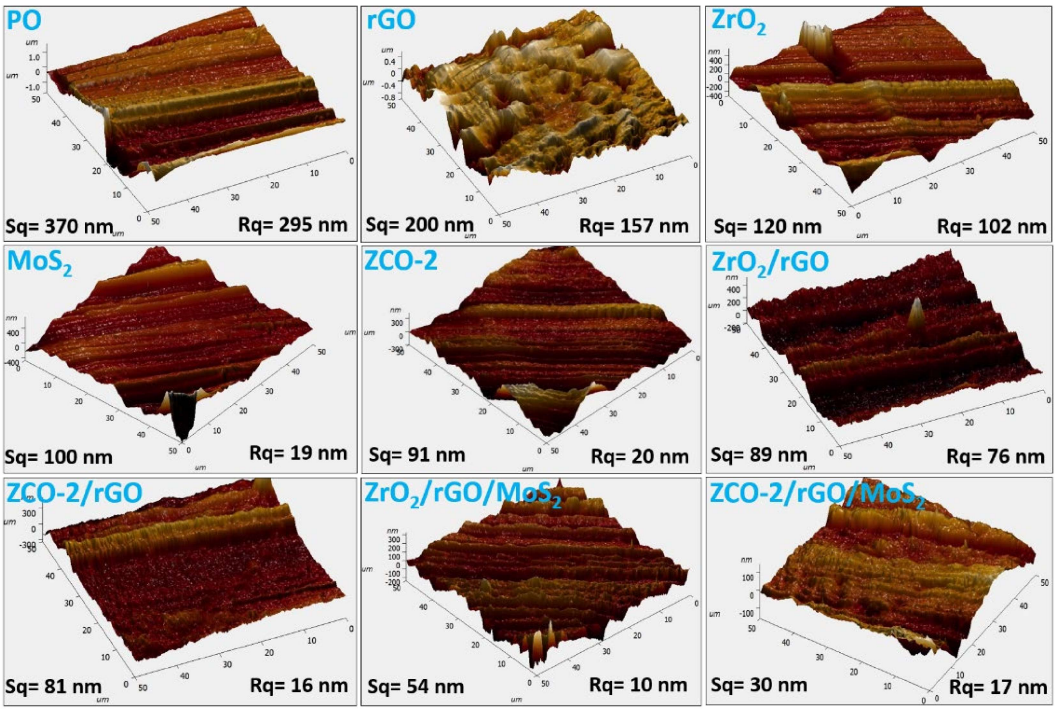

Fig. 5.14. *3D* AFM images of the worn steel surface lubricated with blank paraffin oil (PO) and blends of PO with 0.125% w/v nano additives at 392 N applied load.

It can be noticed that there is a substantial decrease in the values of Rq and Sq from plain paraffin oil to the blends of different investigated nano additives. For example, the Sq value of plain paraffin oil being 370 nm undergoes a 46% reduction in the presence of rGO nanosheets. In contrast, for nanoparticles, reduction exceeds to 68% for ZrO_2 and 75% for ZCO-2. The binary composites ZrO_2/rGO and ZCO-2/rGO bring about a further % reduction in Sq values to 76 and 78, respectively. Finally, surprising results for reduction in Sq values are obtained for the ternary composites ZrO_2/rGO/MoS_2 (85%) and ZCO-2/rGO/MoS_2 (92%). The % reduction in surface roughness justifies the role of binary and ternary

nanocomposites towards enhancing the lubricity of the base oil. The AFM images, thus, validate exactly the order obtained from tribological data and the related SEM images.

5.3.5 Characterization of Tribofilm

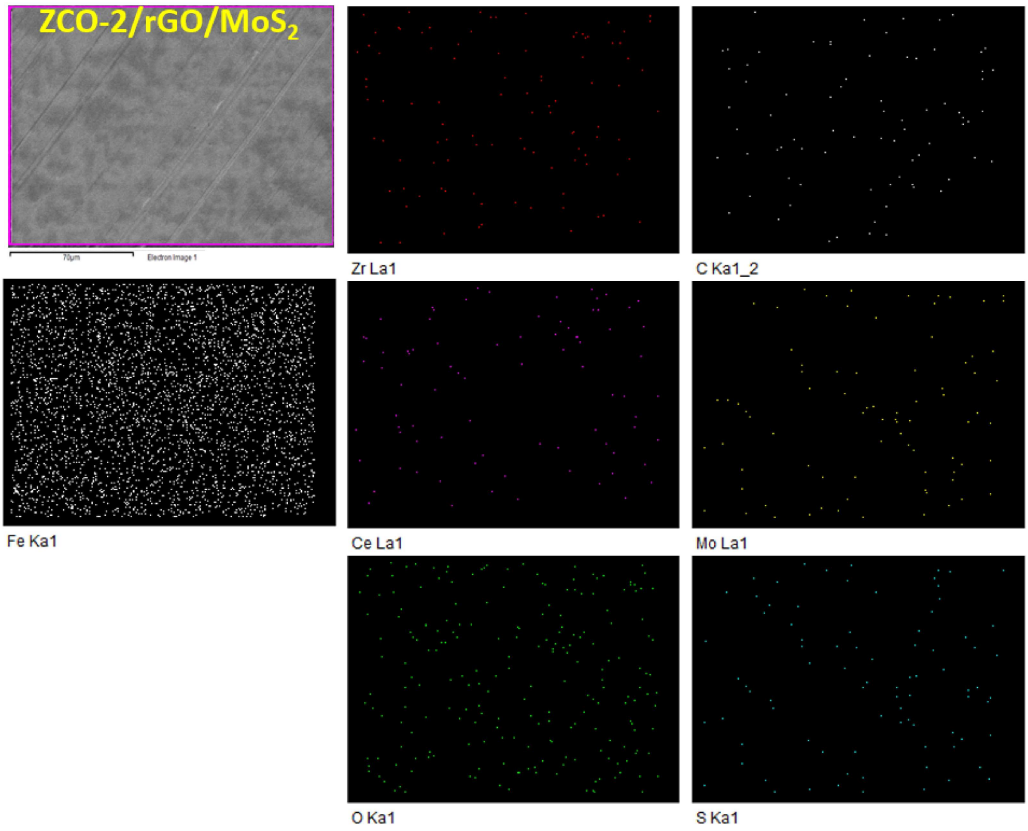

Fig. 5.15. Elemental mapping of worn surface lubricated with a blend of ZCO-2/rGO/MoS_2 nanohybrid in paraffin oil at 392 N applied load.

The elemental mapping and EDX spectra of the tribofilm formed in the presence of a blend of ternary nanohybrid (ZCO-2/rGO/MoS_2) with base oil at 392 N applied load shown in **Fig.**

5.15 and **Fig. 5.16**, respectively, provide information about its elemental composition. Besides the peaks in base oil (**Fig. 5.15a**), some additional peaks due to zirconium, cerium, molybdenum, and sulfur are also observed in **Fig. 5.15b** related to ternary nanohybrid indicating the constituents of tribofilm.

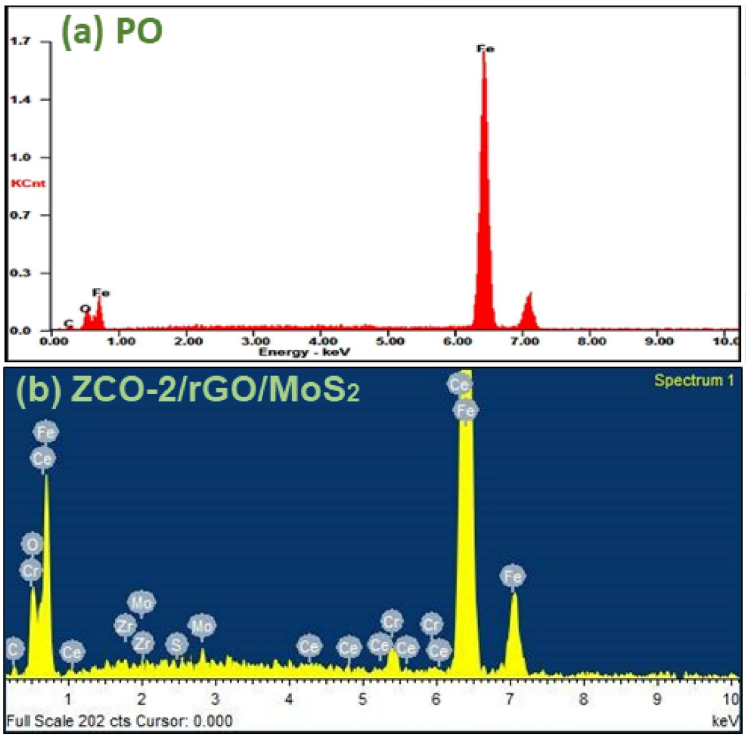

Element	At %
C K	16.74
O K	21.14
Fe K	62.12
Total	100

Element	At %
C K	3.29
O K	8.75
S K	1.09
Cr K	2.18
Fe K	80.09
Zr L	0.80
Mo L	3.60
Ce L	0.20
Total	100

Fig. 5.16. EDX spectra of worn surface lubricated with (a) Blank Paraffin oil (PO) and (b) PO blended with 0.125% w/v ZCO-2/rGO/MoS_2 nanohybrid at 392 N applied load.

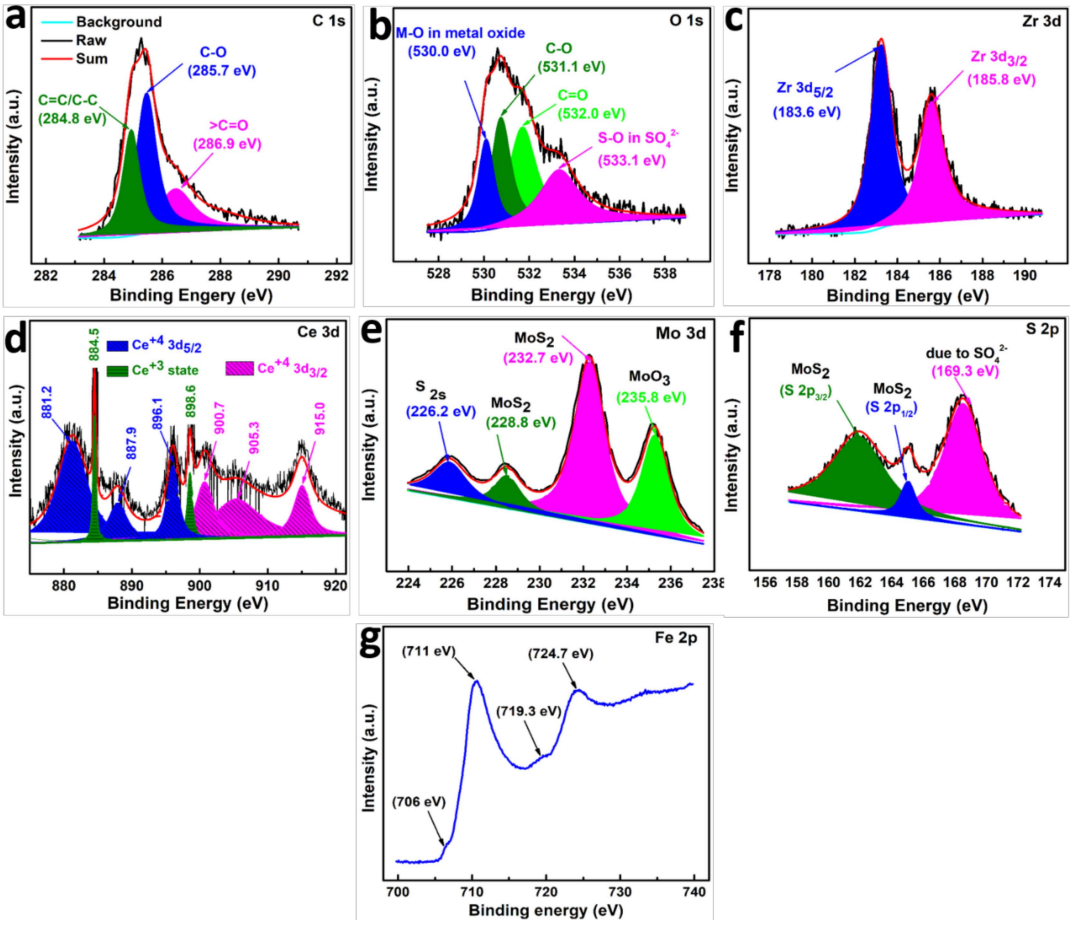

Fig. 5.17. XPS spectra of the worn surface lubricated with ZCO-2/rGO/MoS_2 nanocomposite: (a) C 1s, (b) O 1s, (c) Zr 3d, (d) Ce 3d, (e) Mo 3d, (f) S 2p and (g) Fe 2p spectra.

XPS studies have been conducted to identify the chemical states of different elements in the tribofilm lubricated with ternary composite ZCO-2/rGO/MoS_2. Use has been made of XPS peak fit software to deconvolute the core level spectra. **Fig. 5.17a** exhibits core level spectrum of C 1s deconvoluted into three peaks for C=C, C-O, and C=O bonds with

corresponding binding energies 284.8, 285.7, and 286.9 eV, respectively Zhang et al. 2017, Verma et al. 2019, Zhou et al. 2015]. The spectrum of O 1s displayed in **Fig. 5.17b** shows three peaks. The peaks at 530.0, 531.1, 532.0, and 533.1 eV are indexed for M-O bonds of metal oxides [Zr(IV)-O, Ce(IV)/Ce(III)-O and Fe(II/III)-O], C-O, C=O and –S(VI)-O bond of SO_4^{2-}, respectively [Kim et al. (2004), Zhou et al. (2015), Si et al. (2004), Xu et al. (2019]. The appearance of two peaks at 183.6 and 185.8 eV in the spectrum of Zr 3d (**Fig. 5.17c**) assignable to Zr $3d_{5/2}$ and Zr $3d_{3/2,}$ respectively confirmed Zr in +4 state [Zhou et al. (2015)].

The presence of two sets of peaks in the Ce 3d XPS spectrum (**Fig. 5.17d**) signifies the presence of $3d_{3/2}$ and $3d_{1/2}$ states of Ce^{4+}. The peaks with maxima at 900.7, 905.3, and 915 eV correspond to Ce^{4+} $3d_{3/2,}$ whereas those at 881.2, 887.9, and 896.1 eV are ascribed to Ce^{4+} $3d_{5/2}$. Besides these peaks, two extra peaks with the extremely small area are observed at 884.5 and 898.6 eV, which may be attributed to traces of Ce^{3+} [Kim et al. (2004), Si et al. (2004)].

The intense peaks at 228.2 and 231.3 eV in Mo 3d spectrum (**Fig. 5.17e)** are accorded with Mo $3d_{5/2}$ and Mo $3d_{3/2,}$ respectively. The additional peaks at 226.2 and 235.8 eV are ascribed to S 2s of MoS_2 and Mo-O of $MoO_{3,}$ respectively [Song et al. (2019), Yi et al. (2019), Xu et al. (2017)] Formation of MoO_3 is attributed to oxygen substitution at the defects in MoS_2 nanosheets [Song et al. (2019), Rawat et al. (2019)]. The S 2p spectrum (**Fig. 4.17f)** depicts two peaks of MoS_2 at 162.3 and 163.9 eV for S $2p_{3/2}$ and S $2p_{1/2}$, respectively. Besides these peaks, an additional peak is also identified at 169.3 eV depicting the formation of sulfate [Xu

et al. (2017), Xu et al. (2019)] The binding energies of Mo 3d and S 2p agree very well with the reported values for 2D MoS_2 indicating chemical states as Mo^{4+} and S^{2-} [Yi et al. (2018)]. The Fe 2p spectrum (**Fig. 5.17g)** reveals Fe $2p_{3/2}$ and Fe $2p_{1/2}$ peaks of Fe_2O_3 at 711 and 724.7 eV, respectively. Xu et al. (2019) have shown that the peak at 724.7 eV also corresponds to iron sulfate. Besides, extremely weak peaks at 706, 719.3 eV denote that Fe is almost absent in the native state [Xu et al. (2019)]. Thus, from XPS studies of the worn surface lubricated with the ternary composite ZCO-2/rGO/MoS_2, it may be inferred that all the contents of the tribofilm, including the organic residue of rGO, which is adsorbed on the surface, metal oxides, MoS_2, and products of tribo-reaction like iron sulfate, Fe_2O_3 and MoO_3 have synergistically cooperated yielding illustrious tribological performance of the ternary composite [Zhao et al. (2016)].

5.3.6. Tribo-Chemistry and Mechanism of Lubrication

Based on the above analytical data and discussion thereof, it may be deduced that compatibility of the investigated additives as antiwear agents is attributed to their adherence on the surface of the tribo-pairs, which eventually leads to the formation of tribofilm under standard test conditions. The strong, persistent tribofilm formed *in situ* carries the load. The nature of tribofilm, in fact, plays a decisive role in the overall efficiency of the additives. The inconceivable efficiency of binary /ternary nanohybrids may be explained by invoking synergistic interaction between the individual components. The MoS_2 and rGO have mutually assisted each other during lubrication by maintaining their layered structures instead

of getting smashed into small particles [Nautiyal et al. (2019), Xu et al. (2017)] The presence of rGO helps in preventing the oxidation of MoS_2 into MoO_3 or sulfate [Zhai et al. (2017), Xu et al. (2017)].

Indubitably, the layered structure of rGO and MoS_2 has facilitated sliding motion whereas nanoparticles anchored between nanosheets have acted as spacers [Paul et al. (2019), Bai et al. (2014), Zhou et al. (2015)], and palliated their re-stacking [Zhang et al. (2017), Song et al. (2019), Yi et al. (2018), Paul et al. (2019), Bai et al. (2014), Zhou et al. (2015)]. Besides this, nanoparticles strengthened the nanosheets, prevented agglomeration, and increased their dispersibility [Nautiyal et al. (2019), Song et al. (2019), Bai et al. (2014), Zhou et al. (2015)]. They have also contributed towards improving poor adherence of rGO [Jaiswal et al. (2016)]

Conversely, agglomeration of nanoparticles is also attenuated simultaneously by nanosheets. There is a possibility that these nanoparticles might have acted as nano bearings between nanosheets as well as proximal surfaces to reduce friction [Rawat et al. (2019), Song et al. (2019), Hou et al. (2015), Paul et al. (2019), Tang et al. (2014), Uflyand et al. (2019)] Thus, sliding motion is further facilitated, and lubrication is upgraded. Improvement of lubrication by nanoparticles is also achieved through their tribo-sinterization on the mating surfaces [Rawat et al. (2019), Paul et al. (2019), Tang et al. (2014), Uflyand et al. (2019), Battez et al. (2008)]. Consequently, small pits formed on the surface are restored by nanoparticles by mending mechanism [Rawat et al. (2019), Paul et al. (2019), Tang et al. (2014), Uflyand et al. (2019), Battez et al. (2008)]. The polishing effect of nanoparticles on

the abraded surface is also important in enhancing lubrication [Tang et al. (2014), Uflyand et al. (2019)]. A combination of the above mechanisms has provided the excellent tribological performance of the nanocomposites [Paul et al. (2019)].

The presence of ZrO_2 has provided hardness and toughness to the composite structure and assisted in enhancing its load-bearing capacity. The use of cerium doped zirconia nanoparticles has yielded better results as compared to zirconia nanoparticles themselves. The EDX and XPS studies of the wear scar surface lubricated with the best additive, ZCO-2/rGO/MoS_2 nanohybrid, have provided elemental composition and the chemical form of the constituents. The tribofilm, composed of adsorbed rGO, MoS_2, zirconia, ceria, and the products of tribochemical reactions, Fe_2O_3, MoO_3, and iron sulfate, facilitates lubrication [Xu et al. (20170, Xu et al. (2015), Zhao et al. (2016)]. The MoO_3, a soft material formed after tribo-oxidation, helps in the adherence of the MoS_2 nanosheets on the surface [Xu et al. (2017), Zhao et al. (2016)]. The iron sulfate enhances the capacity of adsorption of the nanosheets on the sliding surfaces, thus decreasing the shearing force and boosting the lubrication [Zhao et al. (2016)].

5.4. Conclusions

The nanoparticles of zirconia (ZrO_2) and 10, 20, and 30% cerium doped zirconia (ZCO-1, ZCO-2, and ZCO-3, respectively) were prepared by the auto-combustion method. The rGO prepared by modified Hummer's method was used to synthesize binary nanohybrids of zirconia (ZrO_2/rGO) and 20% cerium doped zirconia (ZCO-2/rGO). Since 10 and 30%

cerium doped zirconia yielded relatively poor results in tribology test, their nanocomposites were not prepared. Further, MoS_2 nanosheets were prepared by hydrothermal method using ammonium heptamolybdate. These nanosheets were used to prepare ternary nanohybrids ZrO_2/rGO/MoS_2 and ZCO-2/rGO/MoS_2 with the help of the microwave. The as-prepared nanosheets, nanoparticles, and nanocomposites have been characterized by the state of the art techniques such as Raman, FT-IR, SEM/HR-SEM with EDX, TEM/HR-TEM, and powder XRD. The constituents of the nanohybrids are bonded to each other by the non-covalent type of interactions. The dispersions of nanohybrids in the base lube were tested for stability using UV/visible spectroscopy and were found to be almost stable even beyond 48 hours. The tribological activity of the synthesized additives in base oil has been examined based on parameters, MWD, COF, load-carrying capacity, and wear rates gathered from ASTM D4172 and ASTM D5183 tests using four-ball tribo-tester at the optimized concentration, 0.125% w/v. The activity of different additives in paraffin oil was obtained to endorse the order mentioned below-

ZCO-2/rGO/MoS_2 > ZrO_2/rGO/MoS_2 > ZCO-2/rGO > ZrO_2/rGO > ZCO-2 > MoS_2 > ZrO_2 > rGO > PO

From the above studies, it is clear that the tested nanoparticles and nanosheets exhibit sufficiently good tribo-activity. Nevertheless, the activity inflates when binary nanohybrids are tested. In the case of ternary nanohybrids, the activity data surmounts all other additives. Unquestionably, strong synergistic interaction between nanoparticles and nanosheets has

rendered such a high order of activity. The SEM and AFM studies of the worn surface validate the given order. Based on XPS studies, a plausible mechanism of lubrication includes the formation of tribofilm composed of adsorbed rGO, MoS_2, zirconia, ceria, and the products of tribochemical reactions, Fe_2O_3, MoO_3, and iron sulfate. Thus, the ternary nanohybrids in general and ZCO-2/rGO/MoS_2, in particular, may be put forward as prospective antiwear and antifriction agents for lubrication systems.